UAB
Universitat Autònoma de Barcelona

Dipòsit digital de documents de la UAB

This is the **accepted version** of the journal article:

Corby, Sacha [et al.]. «Charge Separation, Band-Bending and Recombination in WO3 Photoanodes». *Journal of physical chemistry letters*, Vol. 10, Num. 18 (September 2019), p. 5395-5401 DOI 10.1021/acs.jpclett.9b01935

This version is available at https://ddd.uab.cat/record/338868

under the terms of the IN COPYRIGHT license.

Charge separation, band-bending and recombination in WO_3 photoanodes

Sacha Corby[1], Ernest Pastor[1], Yifan Dong[1], Xijia Zheng[1], Laia Francàs[1], Michael Sachs[1], Shababa Selim[1], Andreas Kafizas[1,2], Artem A. Bakulin[1] and James R. Durrant[2]*

[1]Department of Chemistry, Imperial College London, White City Campus, 80 Wood Lane, London, W12 0BZ, UK
[2]Grantham Institute for Climate Change, Imperial College London, South Kensington, London, SW7 2AZ, UK

*corresponding: j.durrant@imperial.ac.uk

Abstract

In metal oxide-based photoelectrochemical devices, the spatial separation of photogenerated electrons and holes is typically attributed to band-bending at the oxide / electrolyte interface. However, direct evidence of such band-bending impacting upon charge carrier lifetimes has been very limited to date. Herein we use ultrafast spectroscopy to track the rapid relaxation of holes in the space-charge layer and their recombination with trapped electrons in WO_3 photoanodes. We observe that applied bias can significantly increase carrier lifetimes on all timescales from picoseconds to seconds, and attribute this to enhanced band-bending correlated with changes in oxygen vacancy state occupancy. We show that analogous enhancements in carrier lifetimes can be obtained by changes in electrolyte composition, even in the absence of applied bias, highlighting routes to improve photoconversion yields/performance, through changes in band-bending. This study thus demonstrates the direct connection between carrier lifetime enhancement, increased band-bending and oxygen vacancy defect state occupancy.

Light-driven water oxidation is a kinetically challenging reaction, and as such requires holes to be long lived.[1-4] Metal oxides are the most frequently studied material class for both photoelectrochemical and photocatalytic water oxidation. Most models of oxide photoelectrode function assume that charge carrier longevity, and the ability of slow surface chemistry to compete against faster recombination processes, is the product of surface band-bending.[5-7] However, actual studies of the role of band-bending and concomitant space-charge layer (SCL) formation on the dynamics of photogenerated charge carriers at early times are very limited. Long-lived holes (micro-second to second timescales) with lifetimes capable of driving water oxidation catalysis have been observed under anodic bias in several systems.[8-10] However, the yield of these long-lived holes, and thus the final quantum yield for a device, is primarily determined by the efficiency of charge separation that occurs on much faster timescales. Despite many studies of charge carrier dynamics on ultrafast timescales in

such photoanodes, there is, to the best of our knowledge, only one report demonstrating any relation between applied field and carrier lifetime,[11] even with the widely accepted importance of band-bending induced charge separation in most models of photoelectrochemical function. The role of band-bending is also of particular importance, and poorly understood, for particulate photocatalyst systems, which may evolve oxygen without bias and sometimes without scavenger,[12-13] suggesting that electrolyte-induced band-bending alone may be adequate to inhibit recombination processes and enable water oxidation. However, the extent to which either bias- or electrolyte-induced band-bending impacts upon early carrier dynamics, and ultimately device quantum yields, remains unclear.

In this work, we examine the ultrafast kinetics of electrons and holes in nanostructured WO_3 photoanodes, a promising, robust material for solar water oxidation. WO_3, with a band gap of ~2.6 eV, is generally reported to have a high intrinsic doping density as a result of readily formed oxygen vacancy defects.[14-15] These defects manifest as reduced tungsten centres neighbouring sites absent in oxygen, and thus give rise to a characteristic broad W^{5+} absorption at red wavelengths, rising into the near IR.[16-17] There is ongoing discussion in the literature regarding the effects of these states on charge transport and catalysis, with proponents claiming improved conductivity and critics proposing increased trap-mediated recombination.[18-23] These states lie energetically below the conduction band edge, with a fairly large energetic distribution.[17, 24] Recent studies of ultrafast kinetics in WO_3 have shown that the presence of large numbers of such occupied vacancy states results in rapid trapping of photogenerated holes (<0.2 ps after excitation), whereas electrons may trap into unoccupied vacancy states that lie above the Fermi level.[17] Modulation of the occupancy of these states through band-bending has been demonstrated to significantly affect electron extraction timescales,[24] but the relationship between the electronic occupancy of these defect states, the degree of band-bending and the ultrafast dynamics of photogenerated charges has yet to be directly probed.

The WO_3 films used herein were synthesised by aerosol assisted chemical vapour deposition (AA-CVD) to produce nanoneedle structures on FTO with high surface area (see SI for details). These needles have been shown to give good photocurrent onset (0.45 V_{RHE}) and reasonable Faradaic efficiencies for oxygen evolution (~87%).[24] However, despite faster water oxidation kinetics than the other commonly studied transition metal oxides, the maximum photocurrent reported to date for WO_3 under 1 sun irradiance and 1.23 V_{RHE} is only approximately 70% of the 5.3 mA/cm^2 theoretical maximum.[25] This performance is also an outlier, with more publications reporting photocurrents closer to ~10-20% of the theoretical limit, and quantum yields far lower than 1, indicating severe recombination losses.[24, 26-31] Using transient absorption spectroscopy, we demonstrate herein that space-charge layer formation, achieved through electrolyte contact or applied bias in a three electrode cell, can significantly retard the ultrafast recombination processes that largely determine the efficiency of photoelectrochemical and photocatalytic performance.

Figure 1a shows the transient absorption (TA) spectra of WO_3 immersed in electrolyte (0.1 M H_2SO_4) in the absence of applied bias at different time delays after exciting with a 355 nm laser. Two features can be determined: a broad absorption spanning most of the visible region, already present within a picosecond of excitation; and a smaller, slower rising feature that peaks around 500 nm. This feature at 500 nm is not always readily apparent due to the varying degree of overlap of the larger signal and thus we used a global analysis fitting to resolve the two features, shown in Figure 1a (see Supporting Information for details). The more dominant feature at long wavelengths we assign to electrons localised at W^{5+} centres. This assignment agrees with previous spectral studies on slower timescales.[24, 32] Furthermore, this spectral range corresponds to the W^{5+} absorption observed in steady-state studies, and typically assigned to W^{5+} species localised adjacent to oxygen vacancies.[33-35] We associate the second feature at 500 nm with reactive holes in WO_3, as also supported by previous kinetic studies on longer timescales.[24, 32] Both species can be identified within picoseconds of excitation and are followed herein until the timescales of reaction and extraction (see below). For further confirmation of these optical assignments, we turned to spectroelectrochemistry (Figure 1b). With the spectrum at open circuit potential taken as reference (OCP, ~0.5 V_{RHE}), the space-charge layer (SCL) width was altered using anodic and cathodic variations in potential, resulting in the respective loss and gain of a broad feature at longer wavelengths. This feature, previously reported in photo- and electrochromic studies of WO_3, arises from W^{5+} states associated with oxygen vacancies, and therefore highlights that the occupancy of these states and the degree of band-bending in WO_3 are directly correlated.[34, 36-37] The clear resemblance between the spectral signal observed when a greater number of these states are occupied (Figure 1b, cathodic potential) and the broad, red-NIR TA (Figure 1a, red) confirms our assignment of this signal to photogenerated electrons in W^{5+} states, and thereby indicates their trapped nature. As such, this correlation suggests that changes in oxygen-vacancy state occupancy as a result of band-bending may also manifest in changes in photogenerated populations that can be monitored transiently, with likely repercussions for performance.

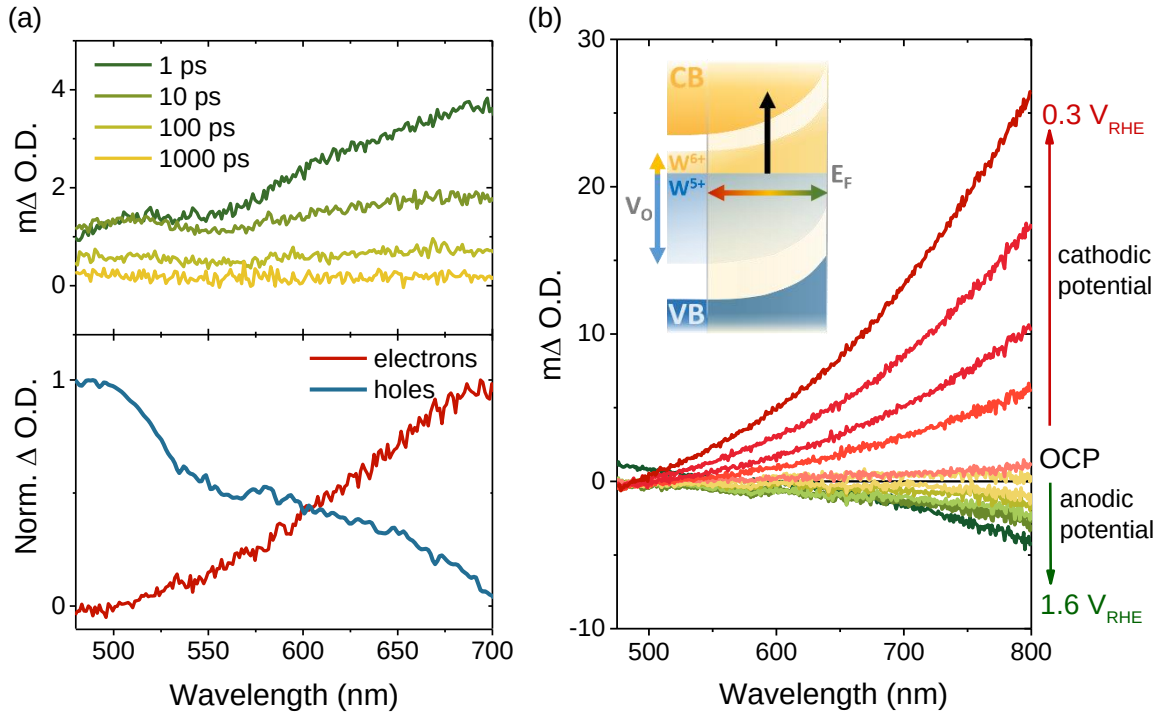


Figure 1: Spectral characterisation of WO_3, resolving features that correspond to electrons and holes. (a) TA spectra between 1 ps and 1000 ps (top) and separated electron and hole spectra from global analysis (bottom); no applied bias, 355 nm pump, 0.2 mJ/cm^2. (b) Spectroelectrochemistry with respect to the open circuit potential (OCP), showing the change in oxygen vacancy defect state occupancy with band-bending and the similarity with the TA electron signal. All spectra collected in 0.1 M H_2SO_4. Inset: schematic showing occupied (blue) and unoccupied (yellow) states, the mid-band oxygen vacancy defects (V_O), the absorption probed by the technique (black arrow) and the changing SCL (coloured arrow).

The kinetics of the electrons (measured at 700 nm) and holes (measured at 500 nm) in the absence of applied bias are given in Figure 2a. The figure shows that the TA kinetics at early times are markedly different for both species. The electron signal shows an instrument-limited rise, thus reflecting a population generated immediately after photoexcitation. In contrast, the hole signal shows a build-up within the first 6 ps due to the formation of a new state (see also Figure S5 for further data on this rise). The decay dynamics of both signals overlap at later times, indicating recombination between the two species (Figure 2a). We propose that the early-time decay of the electron signal is primarily associated with bulk electron-hole recombination, whereas the relatively slow rise at 500 nm is tentatively assigned to the relaxation/localisation of holes within the SCL (Figure 2b). This latter assignment stems from two previous observations. Firstly, outside the SCL (or in the absence of one), photogenerated holes rapidly trap into occupied oxygen vacancy states, resulting in

a bleached signal over the W^{5+} absorption range,[17] consistent with the rapid initial decay at 700 nm in Figure 2a indicative of a loss of electron absorption. Secondly, catalytically active holes that absorb at 500 nm have been shown to oxidise water on slower timescales, thereby indicating that this absorption arises from holes localised within the depletion layer.[24] The data shown in Figure 1a and Figure 2b are, in essence, optical evidence for the initial separation of electrons and holes, with distinct optical signals and kinetics observed for both photogenerated species.

It is also apparent from Figure 2a that the early-time TA data present an oscillatory feature on top of the electron and hole signals that dampens with time. This feature, strongest at shorter wavelengths, though present over the entire spectral window (see two-dimensional map, Figure S1), is characteristic of a superposition of optically induced vibronic transitions (vibrations). Figure 2c shows the averaged Fourier transform (FT) of the oscillatory component at two extremes of the TA spectrum. At shorter wavelengths, where hole absorption dominates, we observe two major peaks at ~60 cm^{-1} and 75 cm^{-1}, also observed in the ground state Raman spectrum for WO_3.[38] Similar photoinduced oscillations have been observed in $BiVO_4$ and have been assigned to coherent phonons associated with hole trapping.[39] However, given the electronic proximity of the TA signal to the band-gap, we cannot discard the possibility that these frequencies are due to ground-state vibrational wavepackets. In contrast, at longer wavelengths, we observe a redistribution of peak intensities, with new features below 70 cm^{-1} and at ~100 cm^{-1} (see also Figure S1a-c). Such frequency spread at these wavelengths is suggestive of excited-state vibrational coherences.[40] Though there is scope for further analysis to establish the role of these vibrations in catalytic activity, the strong coupling between the electronic and nuclear degrees of freedom apparent from the observed oscillations is indicative of the relatively localised nature of the photogenerated electrons and holes, consistent with our discussion above.

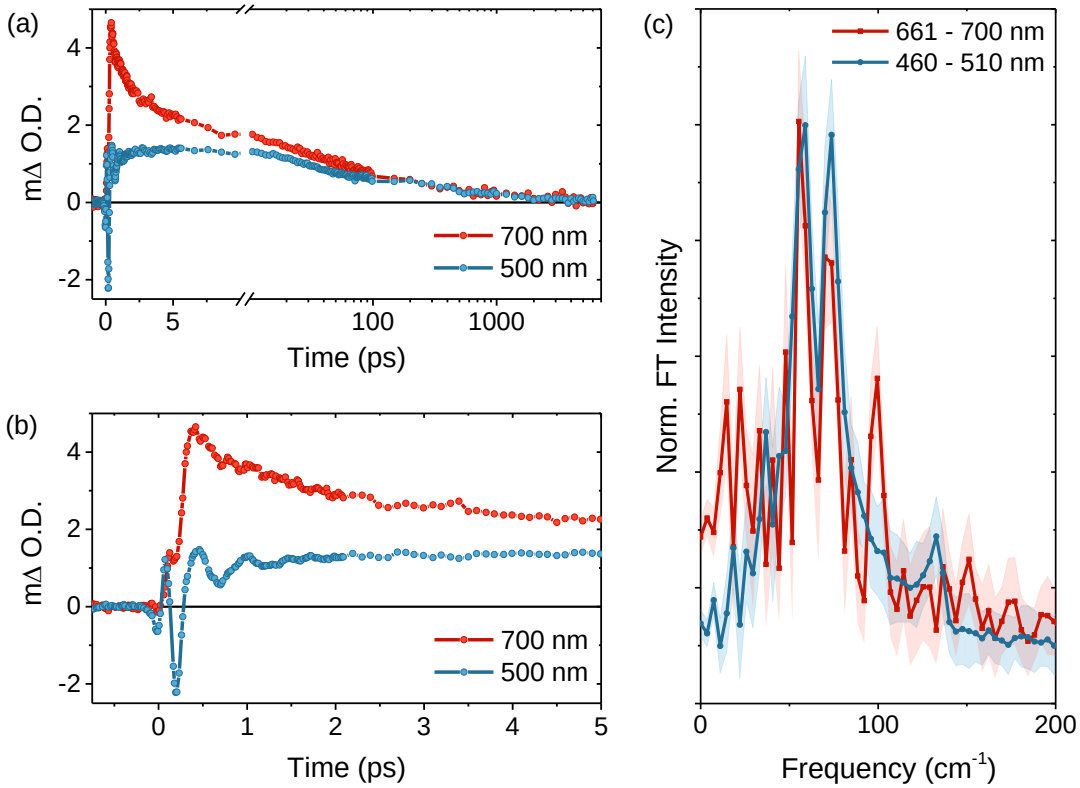


Figure 2: (a) Kinetics of electrons (700 nm, red) and holes (500 nm, blue) recorded from femtoseconds after excitation to 6 nanoseconds and (b) a closer view of the first 5 picoseconds, showing the rise of the hole signal and an oscillatory feature in the signal. (355 nm pump, 0.2 mJ/cm^2) (c) Fourier Transform of the oscillatory feature, showing peaks corresponding to vibrational modes. The faded data gives the 95% confidence interval.

To determine how the degree of band-bending affects charge separation and recombination, we monitored the ultrafast kinetics as a function of applied bias. We found that both the hole (Figure 3a) and electron (Figures 3b) signals become longer lived as the applied potential increases. This change in kinetics was observed to be reversible, and more pronounced with lower excitation densities (see Figure S4). This increase in lifetime can be attributed to an enhancement in the SCL inhibiting recombination processes as band-bending is increased. By taking the half-time of the electron decay at each potential, we find the rate of change is largest at lower potentials, closer to the OCP, where the dependence of SCL width upon applied potential will be strongest (Figure S2). More quantitatively, we find that increase in carrier lifetime with applied bias correlates with the expected increase in SCL thickness, as demonstrated in Figure S2.[41-42] A second effect of anodic bias on the hole signal can be noted in Figure 3a: as well as increasing hole lifetime, applied bias accelerates the initial appearance of the 500 nm hole signal (grey arrow, see Figure S3 for zoom). This trend is consistent with an increase in hole localisation in the broadened SCL. The earlier rise could also result from

the increased field driving photogenerated holes towards the surface faster, though the timescale of the rise suggests the holes we observe are those already in, or very near, the SCL.

When the excitation intensity was increased, a smaller dependency of carrier lifetime on applied field was observed, as illustrated in Figure S4. This observation is likely related to the relative densities (per cm^2) of charge in the SCL compared to the density of photogenerated carriers (4×10^{14} cm^{-2} for excitation conditions used in Figure 3). At high photon fluxes, the photogenerated charge density becomes comparable or larger than the SCL charge density, resulting in screening of the SCL field. Compared to most other metal oxides, WO_3 typically exhibits a higher doping density, associated with a higher number of intrinsic oxygen vacancy states, on the order of 10% of the metal content in these needles (although the electrical doping density will be lower than this chemical doping density).[24] The challenge of undertaking ultrafast TAS experiments at excitation densities lower than the dark doping density is most likely the reason for the general absence of bias dependent kinetic data in literature on other, less doped materials, particularly as excitation fluences are often higher than those employed herein.[43-44] It is likely that stronger bias dependencies would be observed at even lower excitation fluences, more comparable to charge densities generated under solar irradiation, although signal to noise limitations prevented such experiments for the study reported herein.

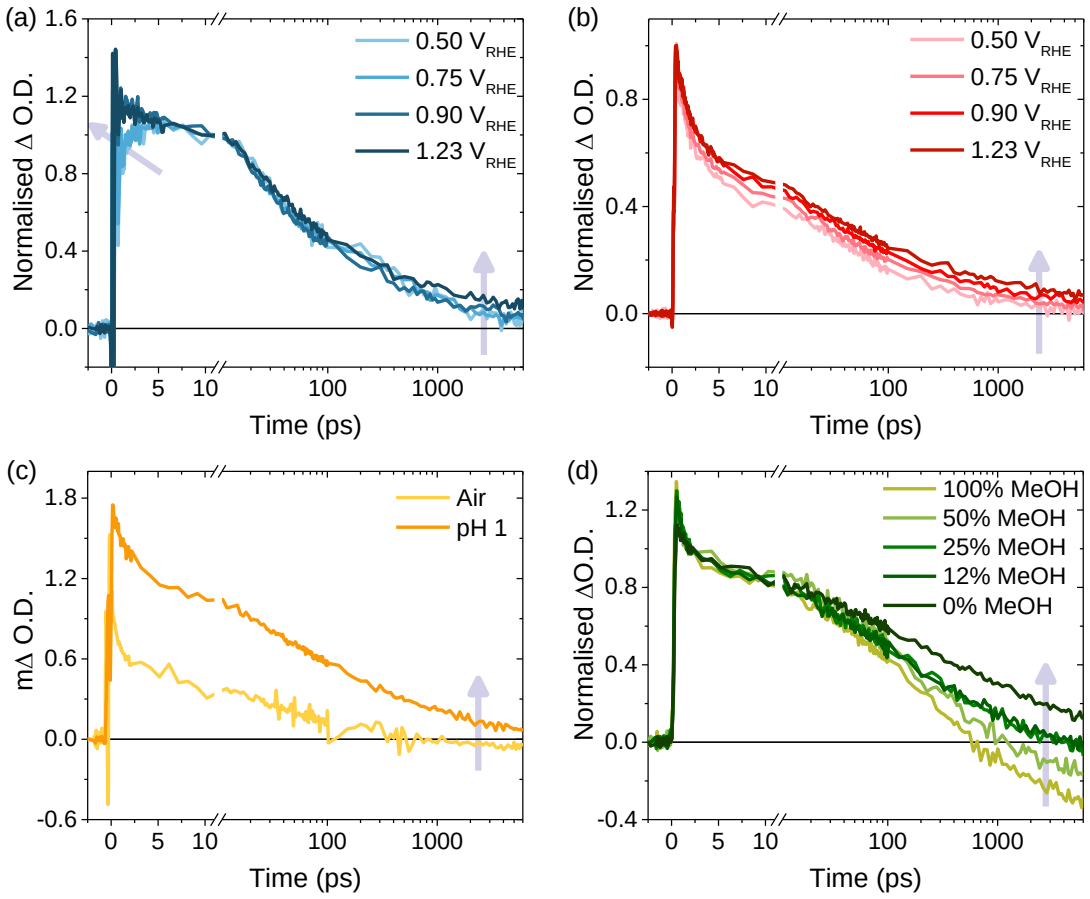


Figure 3: Charge carrier dynamics under different band-bending conditions. The arrows indicate increased carrier lifetime or faster signal rise with increased anodic bias. The kinetics of (a) holes (500 nm) and (b) electrons (700 nm) in 0.1 M H_2SO_4 with increasing applied potential (0.50 – 1.23 V_{RHE}). (c) Electron kinetics in air and in 0.1 M H_2SO_4 and (d) electron kinetics in MeOH with increasing percentage of pH 1 electrolyte (0.1 M H_2SO_4). All data measured with 355 nm pump, 0.2 mJ/cm^2.

As we assign the longer carrier lifetimes observed with anodic bias to increased band-bending, it therefore follows that any method of increasing the space-charge layer should produce a similar result. In particular, immersion of an electrode in electrolyte, even in the absence of applied bias, can result in SCL formation due equilibration of the metal oxide Fermi level with the chemical potential of the electrolyte.[7] Figure 3c shows a comparison of electron decay kinetics for a WO_3 sample in air and when immersed in the 0.1 M H_2SO_4 electrolyte used throughout this work. In electrolyte, a larger, longer-lived electron signal is observed, which we assign to enhanced band-bending causing an improvement in charge separation. Moreover, the enhancement can be considered an increase in the number of unoccupied oxygen vacancy states available to trap electrons, and a reduction in any hole trapping that may occur without a SCL, which would otherwise lower the signal. Electrolyte-induced SCL

formation was confirmed by UV-visible absorption spectra in air and electrolyte, which indicated an electrolyte absorption change reasonably consistent with a loss of W^{5+} states, similar to that shown in Figure 1. (Figure S5). Furthermore, an accelerated appearance of the hole signal at 500 nm is observed in electrolyte compared to air (Figure S6), similar to the effect seen with bias induced band-bending (Figure 3a), and thus provides further evidence of space-charge layer formation. Longer carrier lifetimes in electrolyte were consistently observed for several samples, although the magnitude of the change differed (Figure S7). This is likely due to differences in SCL thickness between samples, which will vary with changes in dark doping density. Oxygen vacancies form the main intrinsic dopants in WO_3 and their concentration and energetic distribution is known to vary with factors such as synthesis temperature.[26, 45]

A similar increase in charge carrier lifetime was observed with changes in the electrolyte composition, shown, for example, in Figure 3d for WO_3 in methanol (MeOH) with added aliquots of 0.1 M H_2SO_4 (pH 1). A faster electron decay is observed in 100% MeOH, with the half-life of the decay increasing as the proportion of pH 1 electrolyte is increased. This suggests that the degree of band-bending following immersion in MeOH is less than in the aqueous pH 1 electrolyte, which may correlate with the less positive redox potential reported for MeOH compared to water.[46-47] At greater MeOH concentrations, the signal at 700 nm becomes negative at longer times (bleaches), which we assign to enhanced hole trapping into occupied oxygen vacancy states, reducing the trapped-electron count at nanosecond timescales to below the *'pre-pump'* original. This interpretation complies with the bleached signal observed at these wavelengths in WO_3 samples with greater concentrations of filled oxygen vacancy-states, which can rapidly trap holes.[17] Figure 3d shows that as the ratio of pH 1 electrolyte to MeOH is increased, electron lifetime increases, consistent with the idea of a greater SCL, which will depopulate potential W^{5+} traps and retard recombination by enhancing charge separation.

Figure 4a plots the electron kinetics measured at 700 nm for different applied potentials from ultrafast timescales up to 1 second (normalised for the difference in excitation conditions used for later times). It is apparent that the increased proportion of long-lived charge carriers observed with more anodic bias on ultrafast timescales correlates well with the improved charge longevity seen at times relevant to catalysis. The magnitude and decay kinetics of 700 nm signal on the millisecond timescale correlate with transient photocurrent measurements of electron extraction (Figure S8), consistent with the assignment to long-lived electrons (and specifically to electrons trapped at oxygen vacancy states).[24] By mapping the increase in charge extracted with anodic bias, we find a dependency strikingly similar to the increase in electron half-time with anodic bias observed on ultrafast times (compare Figure S2 with S8b). Such correlating trends clearly indicate that the positive effects of SCL formation in retarding fast recombination processes are carried through to later times, and, in fact, account for most of the improved performance seen with bias, with strong repercussions on maximum

attainable performance. The kinetics of the charge carriers in WO_3, from generation to reaction and extraction, are summarised in Figure 4b.

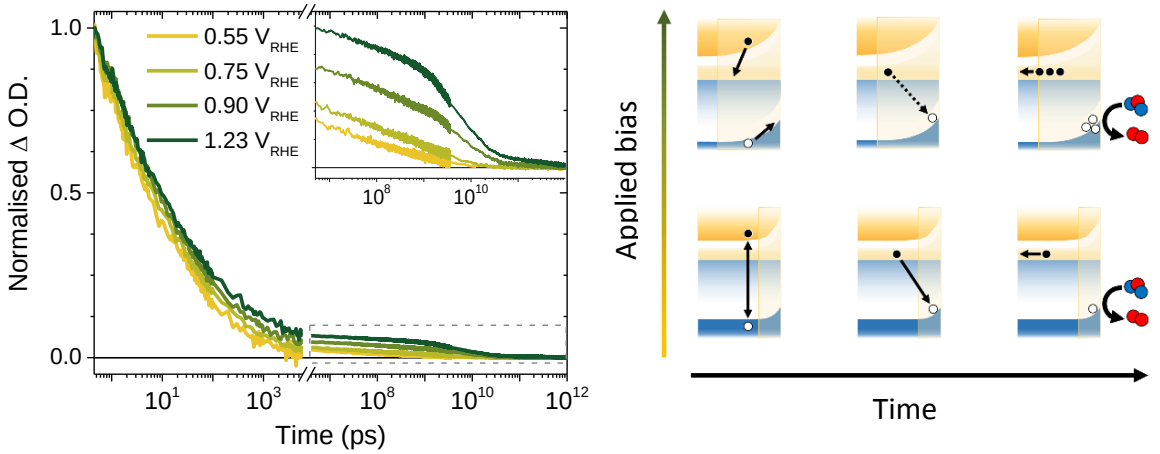


Figure 4: (left) Kinetics of transient optical signal at 700 nm, assigned to electrons, under different applied potentials from 0.5 ps to 1 s. A break in the x-axis between 6 ns and 1 µs is present as those timescales could not be probed (355 nm, 0.2 mJ/cm^2). (right) Schematic representation to describe kinetics in (a), showing charge separation, trapping and recombination timescales relative to those of reaction for WO_3 in 0.1 M H_2SO_4. Black arrows indicate movement of electrons (black circles) and holes (white circles). At early times and low applied bias, bulk recombination dominates and many holes that reach the surface face recombination with bulk electrons before catalysis. With increased applied bias we see improved charge separation at early times, which gives way to less recombination within the SCL (dashed arrow), and a greater photocurrent and performance at later times. Upper is under higher bias, lower is low bias. SCL shown in faded region, blue regions are occupied states, yellow are empty states, with V_O states as shown in Figure 1 inset.

In summary, we have determined that increased space-charge layer formation with applied bias is directly correlated with increased charge carrier lifetimes in WO_3 photoanodes. Often assumed, though never previously directly demonstrated, we have also shown that the space-charge layer formed on contact with electrolyte, in the absence of applied bias, also can increase the lifetime of charge carriers. In this work, we were able to observe separate localisation of electrons and holes from the first few picoseconds, with the former trapped into oxygen vacancy defect states and the latter observed in the SCL. However, this result also highlights that only holes that are localised in the SCL are likely to participate in water oxidation, with most others presumably lost to bulk recombination into W^{5+} states, as observed in the absence of a SCL.[17] This gives a likely rationale for the lower external quantum efficiencies reported for this material,[24, 29] and suggests that tighter control of these defects and their occupancy may significantly boost performance. Analysis of electron kinetics from

generation to extraction reveals the extent of charge loss due to bulk-recombination and the importance of adequate SCL width in inhibiting recombination if greater photocurrents are to be obtained. It is therefore important for the next generation of photoanodes to be engineered such that bulk material is minimised (i.e. adequate nanostructuring), and suitable doping levels are obtained to balance charge transport properties with vital SCL formation. Similarly, control of particulate size in photocatalyst systems to increase the SCL to bulk ratio may also lead to enhanced charge separation, and thus, ultimately, improved catalytic performance.

Acknowledgements

J.R.D, A.A.B and E.P acknowledge financial support from the European Research Council (project Intersolar 291482 and EU Horizon 2020 grant 639750). S.C. would like to thank Imperial College for a Schrödinger Scholarship. L.F. thanks the EU for a Marie Curie fellowship (658270). S.S. thanks the EPSRC for DTP funding. Y.D. acknowledges the Cambridge optoelectronics group for sharing their G.A tool. M.S. thanks the Imperial College President's PhD scholarship scheme and A.K. thanks Imperial College for a Junior Research Fellowship, EPSRC for a Capital Award and the Royal Society for a Research Grant (RSG\R1\180434). A.A.B thanks the Royal Society for a University Research Fellowship.

References

1. Kafizas, A., et al., Water Oxidation Kinetics of Accumulated Holes on the Surface of a Tio2 Photoanode: A Rate Law Analysis. *Acs Catalysis* **2017**, *7*, 4896-4903.
2. Pendlebury, S. R.; Barroso, M.; Cowan, A. J.; Sivula, K.; Tang, J.; Gratzel, M.; Klug, D.; Durrant, J. R., Dynamics of Photogenerated Holes in Nanocrystalline Alpha-Fe2o3 Electrodes for Water Oxidation Probed by Transient Absorption Spectroscopy. *Chem Commun (Camb)* **2011**, *47*, 716-8.
3. Pendlebury, S. R.; Cowan, A. J.; Barroso, M.; Sivula, K.; Ye, J.; Gratzel, M.; Klug, D. R.; Tang, J.; Durrant, J. R., Correlating Long-Lived Photogenerated Hole Populations with Photocurrent Densities in Hematite Water Oxidation Photoanodes. *Energy & Environmental Science* **2012**, *5*, 6304-6312.
4. Upul Wijayantha, K. G.; Saremi-Yarahmadi, S.; Peter, L. M., Kinetics of Oxygen Evolution at A-Fe2o3 Photoanodes: A Study by Photoelectrochemical Impedance Spectroscopy. *Physical Chemistry Chemical Physics* **2011**, *13*, 5264-5270.
5. Peter, L. M., Energetics and Kinetics of Light-Driven Oxygen Evolution at Semiconductor Electrodes: The Example of Hematite. *Journal of Solid State Electrochemistry* **2012**, *17*, 315-326.
6. Hisatomi, T.; Kubota, J.; Domen, K., Recent Advances in Semiconductors for Photocatalytic and Photoelectrochemical Water Splitting. *Chem Soc Rev* **2014**, *43*, 7520-35.
7. Zhang, Z.; Yates, J. T., Band Bending in Semiconductors: Chemical and Physical Consequences at Surfaces and Interfaces. *Chemical Reviews* **2012**, *112*, 5520-5551.

8. Cowan, A. J.; Durrant, J. R., Long-Lived Charge Separated States in Nanostructured Semiconductor Photoelectrodes for the Production of Solar Fuels. *Chemical Society Reviews* **2013**, *42*, 2281-2293.
9. Cummings, C. Y.; Marken, F.; Peter, L. M.; Upul Wijayantha, K. G.; Tahir, A. A., New Insights into Water Splitting at Mesoporous A-Fe2o3 Films: A Study by Modulated Transmittance and Impedance Spectroscopies. *Journal of the American Chemical Society* **2012**, *134*, 1228-1234.
10. Klahr, B.; Gimenez, S.; Fabregat-Santiago, F.; Bisquert, J.; Hamann, T. W., Photoelectrochemical and Impedance Spectroscopic Investigation of Water Oxidation with "Co–Pi"-Coated Hematite Electrodes. *Journal of the American Chemical Society* **2012**, *134*, 16693-16700.
11. Pendlebury, S. R.; Wang, X.; Le Formal, F.; Cornuz, M.; Kafizas, A.; Tilley, S. D.; Grätzel, M.; Durrant, J. R., Ultrafast Charge Carrier Recombination and Trapping in Hematite Photoanodes under Applied Bias. *Journal of the American Chemical Society* **2014**, *136*, 9854-9857.
12. Maeda, K.; Teramura, K.; Lu, D.; Takata, T.; Saito, N.; Inoue, Y.; Domen, K., Photocatalyst Releasing Hydrogen from Water. *Nature* **2006**, *440*, 295-295.
13. Maeda, K.; Domen, K., New Non-Oxide Photocatalysts Designed for Overall Water Splitting under Visible Light. *The Journal of Physical Chemistry C* **2007**, *111*, 7851-7861.
14. Zheng, H.; Ou Jian, Z.; Strano, M. S.; Kaner, R. B.; Mitchell, A.; Kalantar-Zadeh, K., Nanostructured Tungsten Oxide – Properties, Synthesis, and Applications. *Advanced Functional Materials* **2011**, *21*, 2175-2196.
15. Zhu, T.; Chong, M. N.; Chan, E. S., Nanostructured Tungsten Trioxide Thin Films Synthesized for Photoelectrocatalytic Water Oxidation: A Review. *ChemSusChem* **2014**, *7*, 2974-97.
16. Deb, S. K., Opportunities and Challenges in Science and Technology of Wo3 for Electrochromic and Related Applications. *Solar Energy Materials and Solar Cells* **2008**, *92*, 245-258.
17. Sachs, M., et al., Effect of Oxygen Deficiency on the Excited State Kinetics of Wo3 and Implications for Photocatalysis. *Chemical Science* **2019**, *10*, 5667-5677.
18. Katoh, R.; Furube, A.; Yamanaka, K.-i.; Morikawa, T., Charge Separation and Trapping in N-Doped Tio2 Photocatalysts: A Time-Resolved Microwave Conductivity Study. *The Journal of Physical Chemistry Letters* **2010**, *1*, 3261-3265.
19. Huang, Z. F.; Song, J.; Pan, L.; Zhang, X.; Wang, L.; Zou, J. J., Tungsten Oxides for Photocatalysis, Electrochemistry, and Phototherapy. *Advanced Materials* **2015**, *27*, 5309-5327.
20. Wang, H.; Lindgren, T.; He, J.; Hagfeldt, A.; Lindquist, S.-E., Photolelectrochemistry of Nanostructured Wo3 Thin Film Electrodes for Water Oxidation: Mechanism of Electron Transport. *The Journal of Physical Chemistry B* **2000**, *104*, 5686-5696.
21. Johansson, M. B.; Mattsson, A.; Lindquist, S.-E.; Niklasson, G. A.; Österlund, L., The Importance of Oxygen Vacancies in Nanocrystalline Wo3–X Thin Films Prepared by Dc Magnetron Sputtering for Achieving High Photoelectrochemical Efficiency. *The Journal of Physical Chemistry C* **2017**, *121*, 7412-7420.
22. Johansson, M. B.; Kristiansen, P. T.; Duda, L.; Niklasson, G. A.; Österlund, L., Band Gap States in Nanocrystalline Wo 3 Thin Films Studied by Soft X-Ray Spectroscopy and Optical Spectrophotometry. *Journal of Physics: Condensed Matter* **2016**, *28*, 475802.

23. Liu, G.; Han, J.; Zhou, X.; Huang, L.; Zhang, F.; Wang, X.; Ding, C.; Zheng, X.; Han, H.; Li, C., Enhancement of Visible-Light-Driven O2 Evolution from Water Oxidation on Wo3 Treated with Hydrogen. *Journal of Catalysis* **2013**, *307*, 148-152.
24. Corby, S.; Francàs, L.; Selim, S.; Sachs, M.; Blackman, C.; Kafizas, A.; Durrant, J. R., Water Oxidation and Electron Extraction Kinetics in Nanostructured Tungsten Trioxide Photoanodes. *Journal of the American Chemical Society* **2018**, *140*, 16168-16177.
25. Wang, S.; Chen, H.; Gao, G.; Butburee, T.; Lyu, M.; Thaweesak, S.; Yun, J.-H.; Du, A.; Liu, G.; Wang, L., Synergistic Crystal Facet Engineering and Structural Control of Wo3 Films Exhibiting Unprecedented Photoelectrochemical Performance. *Nano Energy* **2016**, *24*, 94-102.
26. Kafizas, A.; Francàs, L.; Sotelo-Vazquez, C.; Ling, M.; Li, Y.; Glover, E.; McCafferty, L.; Blackman, C.; Darr, J.; Parkin, I., Optimizing the Activity of Nanoneedle Structured Wo3 Photoanodes for Solar Water Splitting: Direct Synthesis Via Chemical Vapor Deposition. *The Journal of Physical Chemistry C* **2017**, *11*, 5983-5993.
27. Ng, C.; Ng, Y. H.; Iwase, A.; Amal, R., Influence of Annealing Temperature of Wo3 in Photoelectrochemical Conversion and Energy Storage for Water Splitting. *ACS Applied Materials & Interfaces* **2013**, *5*, 5269-5275.
28. Apolinário, A.; Lopes, T.; Costa, C.; Araújo, J. P.; Mendes, A. M., Multilayered Wo3 Nanoplatelets for Efficient Photoelectrochemical Water Splitting: The Role of the Annealing Ramp. *ACS Applied Energy Materials* **2019**, *2*, 1040-1050.
29. Rodríguez-Pérez, M.; Rodríguez-Gutiérrez, I.; Vega-Poot, A.; García-Rodríguez, R.; Rodríguez-Gattorno, G.; Oskam, G., Charge Transfer and Recombination Kinetics at Wo3 for Photoelectrochemical Water Oxidation. *Electrochimica Acta* **2017**, *258*, 900-908.
30. Reyes-Gil, K. R.; Wiggenhorn, C.; Brunschwig, B. S.; Lewis, N. S., Comparison between the Quantum Yields of Compact and Porous Wo3 Photoanodes. *The Journal of Physical Chemistry C* **2013**, *117*, 14947-14957.
31. Grigioni, I.; Stamplecoskie, K. G.; Selli, E.; Kamat, P. V., Dynamics of Photogenerated Charge Carriers in Wo3/Bivo4 Heterojunction Photoanodes. *The Journal of Physical Chemistry C* **2015**, *119*, 20792-20800.
32. Pesci, F. M.; Cowan, A. J.; Alexander, B. D.; Durrant, J. R.; Klug, D. R., Charge Carrier Dynamics on Mesoporous Wo3during Water Splitting. *The Journal of Physical Chemistry Letters* **2011**, *2*, 1900-1903.
33. Patel, K. J.; Panchal, C. J.; Kheraj, V. A.; Desai, M. S., Growth, Structural, Electrical and Optical Properties of the Thermally Evaporated Tungsten Trioxide (Wo3) Thin Films. *Materials Chemistry and Physics* **2009**, *114*, 475-478.
34. Li, Y.; Tang, Z.; Zhang, J.; Zhang, Z., Defect Engineering of Air-Treated Wo3 and Its Enhanced Visible-Light-Driven Photocatalytic and Electrochemical Performance. *The Journal of Physical Chemistry C* **2016**, *120*, 9750-9763.
35. Greiner, M. T.; Chai, L.; Helander, M. G.; Tang, W.-M.; Lu, Z.-H., Transition Metal Oxide Work Functions: The Influence of Cation Oxidation State and Oxygen Vacancies. *Advanced Functional Materials* **2012**, *22*, 4557-4568.
36. Su, L.; Dai, Q.; Lu, Z., Spectroelectrochemical and Photoelectrochemical Studies of Electrodeposited Tungsten Trioxide Films. *Spectrochimica Acta Part A: Molecular and Biomolecular Spectroscopy* **1999**, *55*, 2179-2185.
37. Hotchandani, S.; Bedja, I.; Fessenden, R.; Kamat, P., Electrochromic and Photoelectrochromic Behavior of Thin Wo3 Films Prepared from Quantum Size Collodal Particles. *Langmuir* **1994**, *10*, 17-22.

38. Diaz-Reyes, J.; Castillo-Ojeda, R.; Galvan-Arellano, M.; Zaca-Moran, O., Characterization of Wo3 Thin Films Grown on Silicon by Hfmod. *Advances in Condensed Matter Physics* **2013**, *2013*, 9.
39. Aiga, N.; Jia, Q.; Watanabe, K.; Kudo, A.; Sugimoto, T.; Matsumoto, Y., Electron–Phonon Coupling Dynamics at Oxygen Evolution Sites of Visible-Light-Driven Photocatalyst: Bismuth Vanadate. *The Journal of Physical Chemistry C* **2013**, *117*, 9881-9886.
40. Musser, A. J.; Liebel, M.; Schnedermann, C.; Wende, T.; Kehoe, T. B.; Rao, A.; Kukura, P., Evidence for Conical Intersection Dynamics Mediating Ultrafast Singlet Exciton Fission. *Nature Physics* **2015**, *11*, 352.
41. Naatz, H.; Hoffmann, R.; Hartwig, A.; La Mantia, F.; Pokhrel, S.; Mädler, L., Determination of the Flat Band Potential of Nanoparticles in Porous Electrodes by Blocking the Substrate–Electrolyte Contact. *The Journal of Physical Chemistry C* **2018**, *122*, 2796-2805.
42. Regragui, M.; Jousseaume, V.; Addou, M.; Outzourhit, A.; Bernéde, J. C.; El Idrissi, B., Electrical and Optical Properties of Wo3 Thin Films. *Thin Solid Films* **2001**, *397*, 238-243.
43. Huang, Z., et al., In Situ Probe of Photocarrier Dynamics in Water-Splitting Hematite (A-Fe2o3) Electrodes. *Energy & Environmental Science* **2012**, *5*, 8923-8926.
44. Kronawitter, C. X.; Vayssieres, L.; Shen, S.; Guo, L.; Wheeler, D. A.; Zhang, J. Z.; Antoun, B. R.; Mao, S. S., A Perspective on Solar-Driven Water Splitting with All-Oxide Hetero-Nanostructures. *Energy & Environmental Science* **2011**, *4*, 3889-3899.
45. Palgrave, R. G.; Parkin, I. P., Aerosol Assisted Chemical Vapour Deposition of Photochromic Tungsten Oxide and Doped Tungsten Oxide Thin Films. *Journal of Materials Chemistry* **2004**, *14*, 2864-2867.
46. Batista, E. A.; Malpass, G. R. P.; Motheo, A. J.; Iwasita, T., New Mechanistic Aspects of Methanol Oxidation. *Journal of Electroanalytical Chemistry* **2004**, *571*, 273-282.
47. Léger, J.-M., Mechanistic Aspects of Methanol Oxidation on Platinum-Based Electrocatalysts. *Journal of Applied Electrochemistry* **2001**, *31*, 767-771.

For Table of Contents Only

